Medical University and by the Institutional Review Board of Ishinomaki Red Cross Hospital and Sendai Medical Center. Informed consent was obtained from the bereaved family of every patient.

2.2. Immunohistochemical examination

We used the primary antibodies summarized in Table 1. Particularly, the antibodies against D2-40, podoplanin, vascular endothelial growth factor receptor-3 (VEGFR-3), and Prox-1 were used for the detection of lymphatics. For the negative controls for each antibody, mouse isotype-matched monoclonal IgG1 or mouse nonspecific IgG fraction (DAKO Japan), normal goat serum, and normal rabbit serum were used. After blocking with normal serum and incubation with antibodies, the antigen-antibody reaction was visualized by 3,3′-diaminobenzidine tetrahydrochloride. Sections were counterstained by resorcin-fuchsin and hematoxylin.

Dual immunohistochemical staining using CD34 and D2-40, von Willebrand factor, and D2-40 was performed as described previously [24]. Antigen-Antibody reactions were visualized by Vector Red (Vector Laboratories, Burlingame, CA) and 3,3′-diaminobenzidine.

2.3. Morphometry of vascular densities and interstitial area

The numerical density of pulmonary arteries (N_A(PA)) and CD34-positive capillaries (N_A(cap)), the length density of D2-40–positive lymphatic endothelium (L_A(ly)), and the area density of interstitium (A_A(int)) were estimated on overlapping serial sections by a square centimeter grid [25]. Morphometric examinations were performed independently by the 2 pathologists (M.Y. and M.O.).

The degrees to which capillaries, lymphatics, and the volume change of interstitium developed in the lung tissue were quantified in terms of their length density in space (L_V(cap)), the surface density (S_V(ly)), and the volume density (V_v(int)), respectively. These were estimated in a unit area of lung section resorting to basic principles of stereology [25]:

$$L_V(\text{cap}) = 2N_A(\text{cap}) \quad (1)$$

$$S_V(\text{ly}) = 4L_A(\text{ly})/\pi \quad (2)$$

$$V_v(\text{int}) = A_A(\text{int}) \quad (3)$$

Here, N_A(cap), L_A(ly), and A_A(int) are, respectively, the numerical densities of the capillaries, the length density of the lymphatic walls, and the fraction of interstitium, all in terms of area. N_A(cap) was estimated by counting $CD34^+$ capillary number in a grid section of an ocular. L_A(ly) was estimated by measuring the perimeter lengths of the linear profiles of $D2\text{-}40^+$ lymphatics using a projector (V-16C, Nikon, Tokyo, Japan) and a digitizer (Motic Images Plus 2.0S image analysis system).

The shrinkage of existing structures associated with disease progression produces stage-specific deviation. To compare stage-specific data under such deviated conditions, the numerical density, N_A(PA), of muscular pulmonary arteries with an external diameter larger than 100 μm was calculated on the basis of microscopic observations on lung sections, and all the quantitative results denoted as N_A(cap), L_A(ly), and A_A(int) were corrected by dividing by N_A(PA) [26].

2.4. Three-dimensional reconstruction

Reconstruction of 3-dimensional (3-D) images was achieved from 2-dimensional data of serial tissue sections [27]. Briefly, images of lymphatics as D2-40–positive structures were magnified and copied onto tracing paper using a profile projector (V-16C, Nikon). The images on the tracing papers were extracted using a digitizer system (Wacom, Saitama, Japan), and the 3-D image was reconstructed (OZ95; Rose, Sendai, Japan).

2.5. Statistical analysis

The statistical significance of differences between any 2 pairs of the 3 groups was evaluated using Tukey test. A P value less than .05 was considered significant.

3. Results

3.1. Stage-specific histopathologic characteristics of lymphatic and blood vessels in DAD progression

In the exudative stage, characterized by the formation of the hyaline membrane and mild fibrosis (Fig. 1A), greater numbers of capillaries were observed in the alveolar wall than in normal lung (Fig. 1B and C, inset). Lymphatics were observed around large blood vessels and in the lobular septa, as generally observed in a normal lung (Fig. 1C). Hereafter, the lymphatics with these characteristics are termed "existing lymphatics." In the proliferative stage, characterized by the fibrous thickening of the alveolar wall and the presence of intra-alveolar fibrotic lesions (Fig. 1D), lymphatics of various sizes frequently were observed in the lesions, whereas capillaries were undetectable (Figs. 1E and F). Because these lymphatics were observed to emerge in a disease-associated manner, they are termed "newly formed lymphatics" in this article. Heterotopic expression of D2-40 was observed on the surface of the intra-alveolar fibrotic lesions, particularly in the early proliferative stage, although this expression was limited in the later proliferative stage. In the fibrotic stage, characterized by

temporally homogenous remodeling structures that consisted of dense interstitium and enlarged airspaces (Fig. 1G), collapsed capillaries and lymphatics were observed in the interstitium (Fig. 1H, F). The intensity of collagen staining was increased compared with the proliferative stage (Fig. 1G).

Using serial sections, we confirmed the coexpression of other lymphatic markers, namely, podoplanin, VEGFR-3, and Prox-1, on D2-40$^+$ endothelial cells of the newly formed and existing lymphatics (Fig. 2A-F). Other blood vessel markers, such as von Willebrand factor and laminin, were not detected on the D2-40$^+$ cells, indicating that the D2-40$^+$

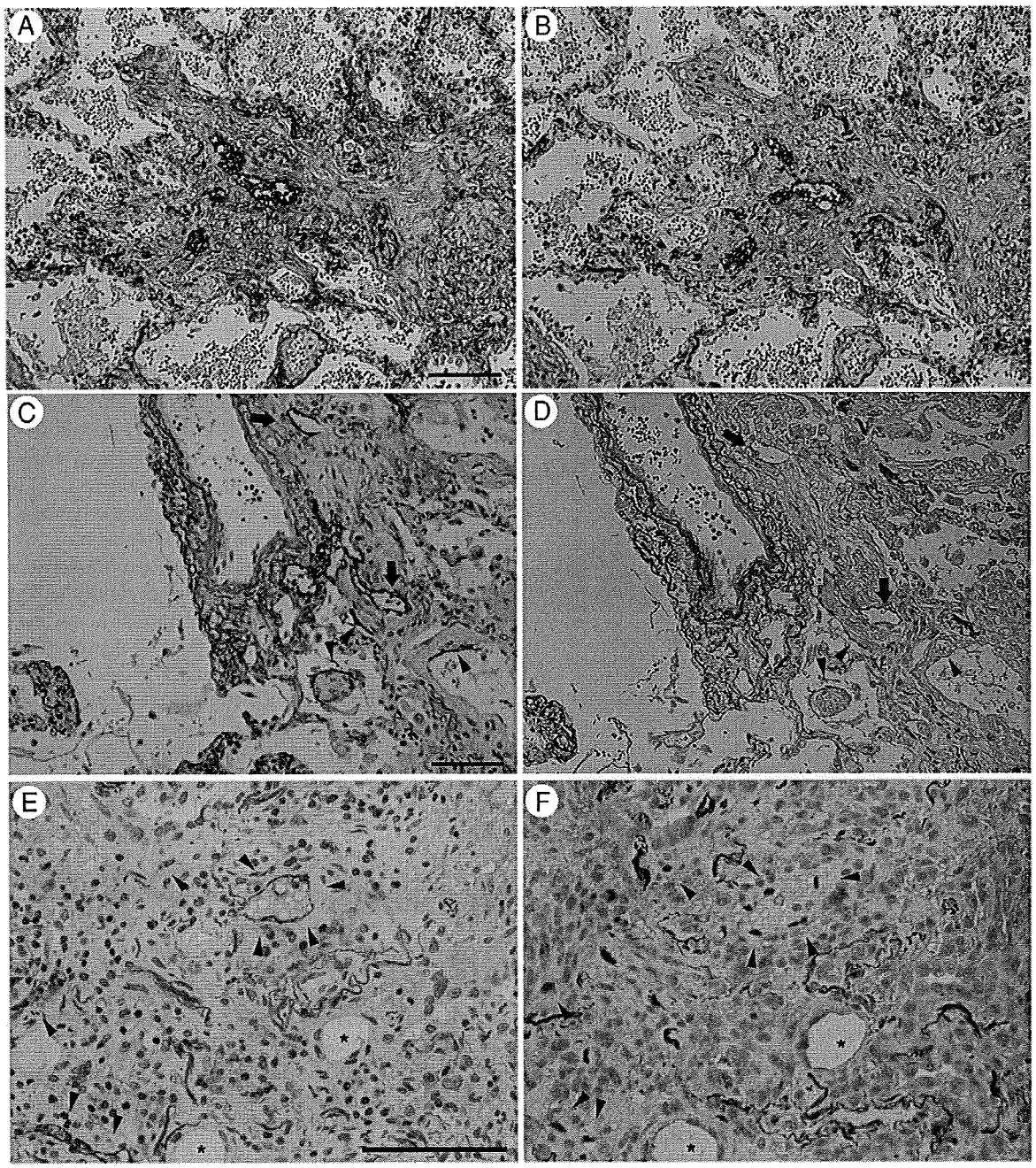

Fig. 2 Colocalization of podoplanin, VEGFR-3, and Prox-1 with D2-40. A and B, Immunostaining of serial sections shows colocalization of (A) D2-40 and (B) podoplanin in both existing and newly formed lymphatic vessels. C and D, Immunostaining of serial sections shows colocalization of (C) D2-40 and (D) VEGFR-3 in both existing and newly formed (arrows) lymphatics. Heterologous colocalization of D2-40 and VEGFR-3 on surface of intra-alveolar fibrotic lesion (arrowheads). E and F, Immunostaining of serial sections shows colocalization of D2-40 (E) and Prox-1 (F) in newly formed lymphatics (arrowheads). Resorcin-fuchsin and hematoxylin for counterstaining. Scale bar, 100 μm.

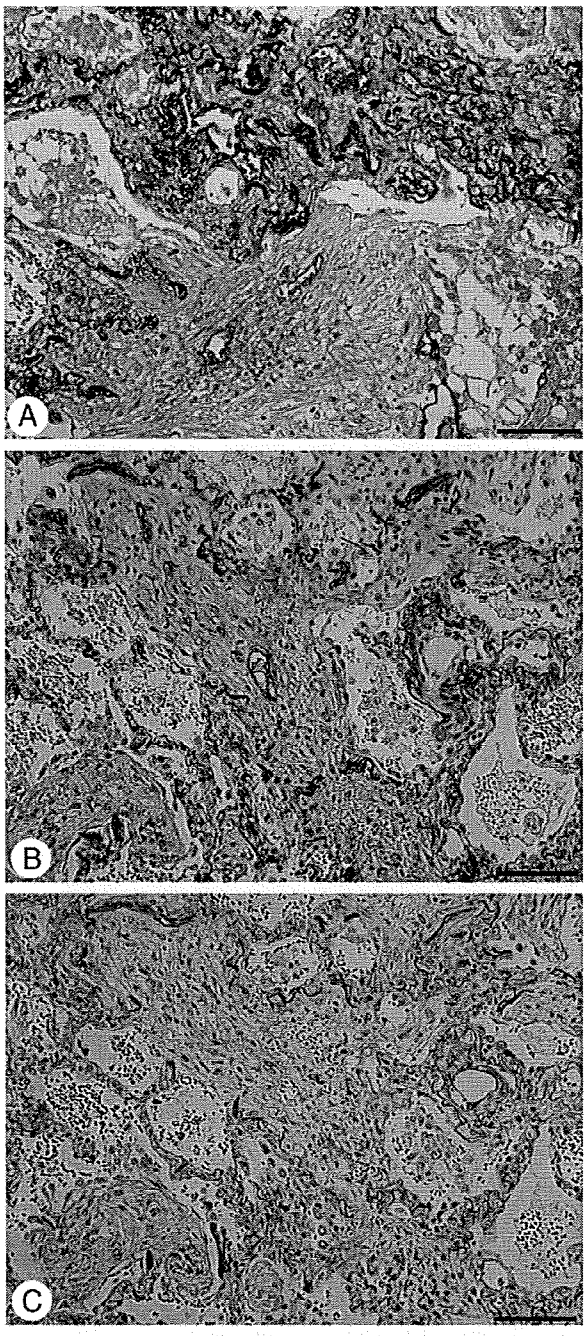

Fig. 3 Dissociated expression of von Willebrand factor (vWF) and laminin from D2-40 expression in intra-alveolar fibrotic lesions. A, Dual immunostaining for vWF and D2-40 counterstained by resorcin-fuchsin and hematoxylin shows that vWF is absent in the intra-alveolar fibrotic lesion, in which D2-40 is expressed. B and C, Immunostaining of serial sections shows that laminin-positive vessels are absent in intra-alveolar fibrotic lesions, where D2-40 is expressed (B), whereas laminin is expressed in a blood vessel (C). Scale bar, 100 μm.

vessels differed from the blood vessels with regard to identifying characteristics (Fig. 3A-C). Neither marker was expressed in the intra-alveolar fibrotic lesions.

3.2. Morphometry analyses

Pulmonary artery density (N_A(PA)), standardized capillary density (N_A(cap)/N_A(PA)), standardized lymphatic density (L_A(ly)/N_A(PA)), and standardized interstitial density (A_A(int)/N_A(PA)) were estimated in normal lungs (n = 4) and DAD in the exudative (n = 5), proliferative (n = 8), and fibrotic (n = 4) stages. The N_A(PA) values in the normal lungs and the 3 stages were 5.3 ± 1.7, 6.3 ± 2.4, 11.3 ± 3.03, and 17.6 ± 3.68/cm^2, respectively (Fig. 4A). The N_A(PA) values in the proliferative and fibrotic stage were significantly higher than that in the previous stage (P < .05). The N_A(cap)/N_A(PA) values in the normal lungs and the 3 stages were 1735.3 ± 484.40, 2679.5 ± 452.57, 3096.6 ± 399.57, and 988.2 ± 338.7, respectively (Fig. 4B). The density in the exudative stage was significantly higher than that in normal lungs (P < .05), whereas the density in the fibrotic stage was significantly lower than that in the proliferative stage (P < .001). These results indicate that the capillary network develops early in or before the exudative stage and regresses in the fibrotic stage. The L_A(ly)/N_A(PA) values of existing lymphatics in the normal lungs and the 3 stages were 5943.2 ± 1581.5, 5503.0 ± 2012.0, 5203.2 ± 1999.6, and 4378.1 ± 916.07, respectively, and the L_A(ly)/N_A(PA) values of newly formed lymphatics were 4068.2 ± 1821.4 and 3796.4 ± 996.45 in the proliferative and fibrotic stages, respectively (Fig. 4C). These findings indicate that the lymphatic network is newly formed exclusively in the proliferative stage, whereas existing lymphatics exist throughout the 3 stages. The A_A(int)/N_A(PA) values in the normal lungs and the 3 stages were 228.9 ± 33.00, 414.5 ± 106.4, 621.4 ± 88.00, and 221.2 ± 60.52, respectively (Fig. 4D). There were statistically significant differences between the normal lungs and the exudative stage, between the exudative and proliferative stages (P < .05), and between the proliferative and fibrotic stages (P < .001).

3.3. Characteristics of newly formed lymphatics in the proliferative stage

Immunohistochemical analyses using serial tissue sections with 3-D reconstruction demonstrated discontinuity between some newly formed and existing lymphatics in the proliferative stage, although some of the new lymphatics connected with existing ones (Fig. 5Aand B). In addition, D2-40 expression on the surface of the intra-alveolar fibrotic lesion continued to the lymphatic lumen (Fig. 5A and B), and further immunohistochemical analysis using serial sections revealed that the surface cells with heterologous D2-40 expression expressed VEGFR-3 but not the epithelial cell marker cytokeratin AE1/AE3 (Figs. 2C and D and 5C and D). In the later proliferative stage, no newly formed lymphatics were

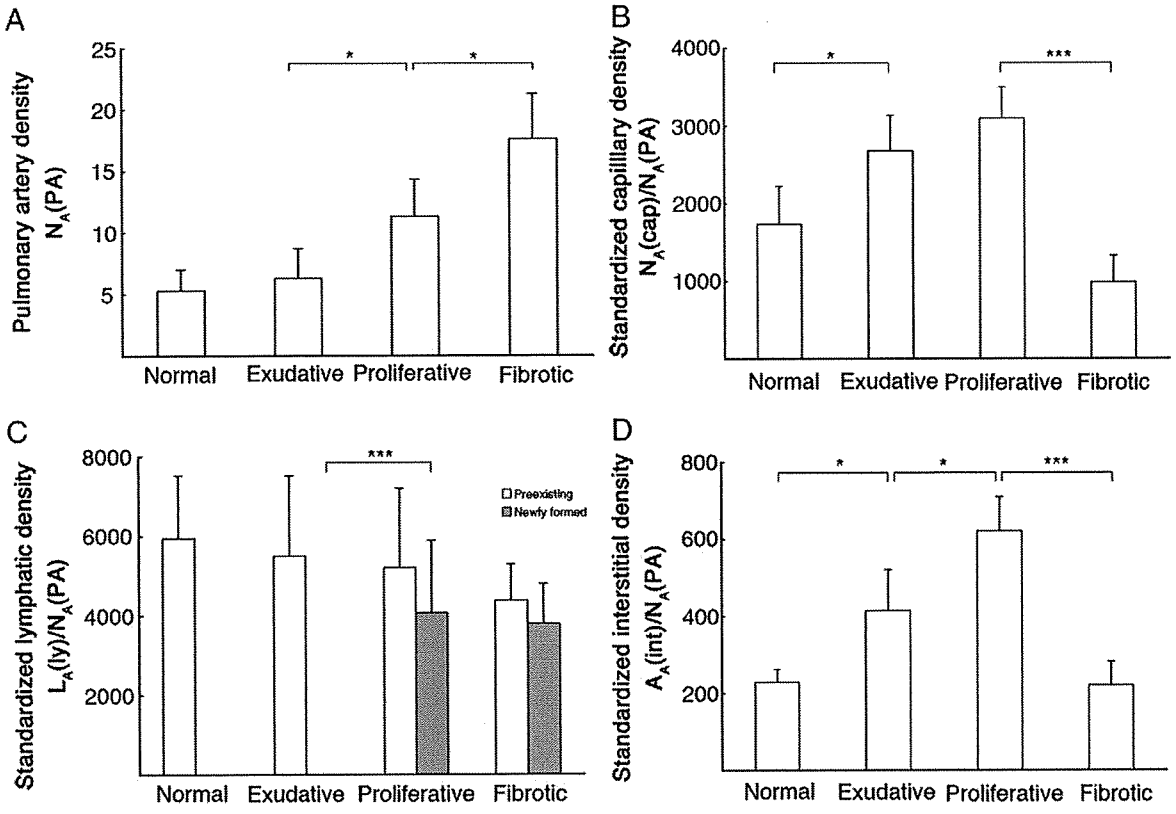

Fig. 4 Morphometry data from specimens in exudative (n = 5), proliferative (n = 8), and fibrotic (n = 4) stages of DAD. Data are shown as mean ± SD. A, Pulmonary artery density: N_A(PA). B, Standardized capillary density: N_A(cap)/N_A(PA). C, Standardized lymphatic density: L_A(ly)/N_A(PA). D, Standardized interstitial density: A_A(int)/N_A(PA). $^*P < .05$; $^{**}P < .01$; $^{***}P < .001$.

observed in the intra-alveolar fibrosis without connection to existing ones (Fig. 6A-C).

4. Discussion

The present study confirmed stage-specific characteristics during the progression of idiopathic DAD, particularly with regard to lymphangiogenesis and capillary angiogenesis. The results lead to new insights, revealing that robust lymphangiogenesis occurs in intra-alveolar fibrotic lesions in the proliferative stage of DAD. On the other hand, capillary angiogenesis was observed to occur early in the exudative stage and subsided thereafter. Notably, capillary angiogenesis was induced to a limited extent in the intra-alveolar fibrotic lesions. In the fibrotic stage, it was evident that blood vessels regress while lymphatics persist. There is limited information regarding the role of the lymphatic system in pathological fibrosis. Our present findings shed new light on this role and will facilitate further investigations into the differential roles of lymphangiogenesis and capillary angiogenesis in pulmonary fibrosis.

The temporal and anatomic correlation of lymphangiogenesis and capillary angiogenesis has been demonstrated in animal models of cutaneous wound healing and bronchitis with *Mycoplasma pulmonis* infection [22,28]. Under these conditions, capillary angiogenesis preceded lymphangiogenesis, and new lymphatics sprouted from existing ones. Proliferation eventually resulted in an intertwined structure of blood and lymphatic vessels; however, this structure regressed in the late stage of wound healing. These findings suggest the significance of the temporal and anatomic correlation of lymphangiogenesis and capillary angiogenesis and the regression of this structure for the completion of wound healing. In the case of DAD, although lymphangiogenesis follows capillary angiogenesis, new lymphatics are formed mainly in the intra-alveolar fibrotic lesions, where blood vessels are absent, and these newly formed lymphatics are anatomically separated from the capillary network. It also is characteristic that lymphatics persist in the fibrotic stage. Matsui et al [29] reported a relatively high density of lymphatics in an experimental renal fibrosis model in rats; the density of the blood vessels was significantly decreased in this area compared with that in a normal interstitial region. In a normal kidney, the presence of lymphatics is restricted to the regions around the interlobular arteries. A lymphatic-dominant lesion in the kidney may be established by lymphangiogenesis in the absence of both preceding capillary angiogenesis and eventual lymphatic regression,

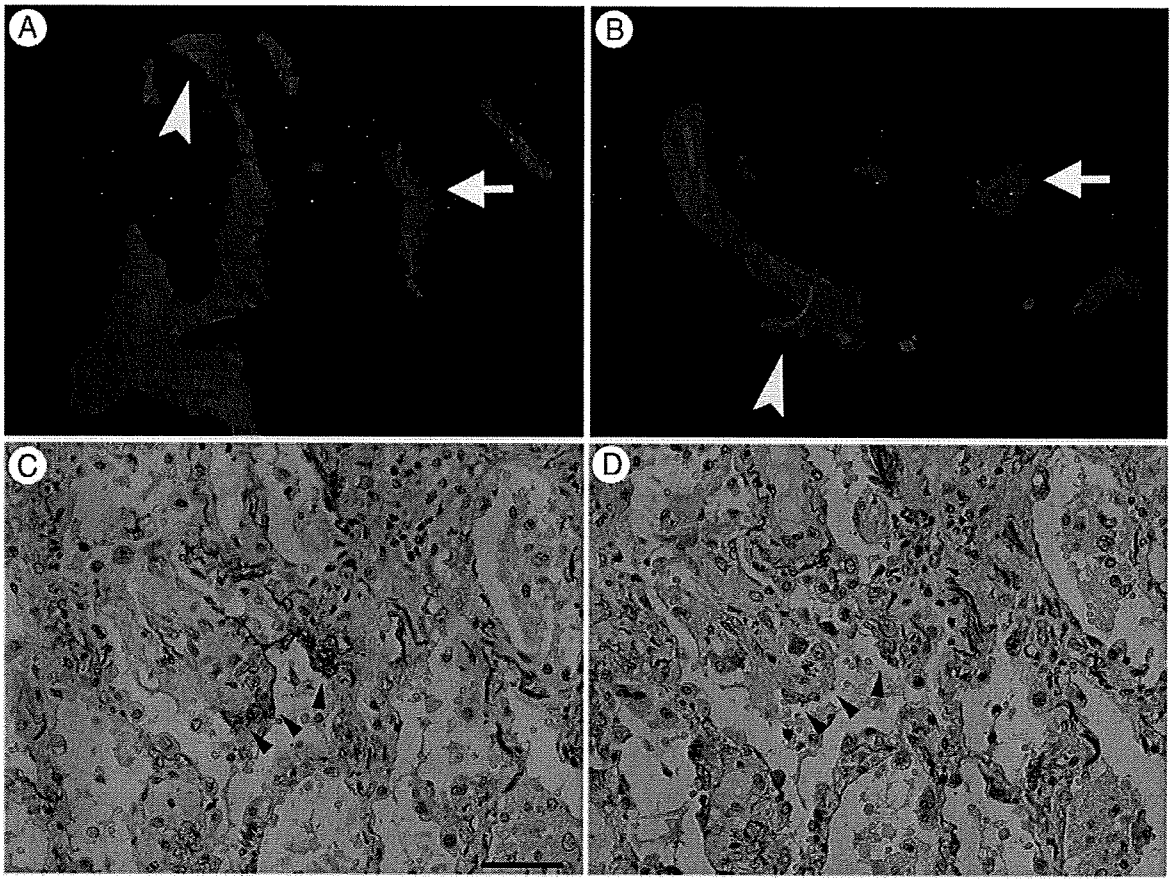

Fig. 5 Characteristics of lymphatic structures in proliferative stage of DAD. Overhead (A) and lateral (B) views of D2-40$^+$ structure revealed by 3-D reconstruction show isolated lymphatic structure from existing lymphatics (arrows) and continuation between surface expression of D2-40$^+$ on intra-alveolar fibrotic lesions and lymphatic vessel in this lesion (arrowheads). The 3-D images are reconstructions of 50 slices encompassing 200-μm thickness of lung tissue. C and D, Serial sections show that D2-40$^+$ cells (arrowheads in panel C) heterologously present on surface of intra-alveolar fibrotic lesions are not colocalized with cytokeratin-positive cells. Scale bar, 100 μm.

as in our cases. It is an important question whether the presence of lymphatic-dominant lesions is characteristic of irreparable fibrosis.

By morphometry analysis, the standardized interstitial density was decreased significantly in the fibrotic stage. The gross evaluation of the intensity of collagen staining revealed that collagen density in a representative lesion was increased remarkably compared with the proliferative stage. These observations imply that the lymphatics persisting in the fibrotic stage of DAD may contribute to the decrease in the standardized interstitial density via fluid drainage. This function may eventually facilitate the architectural remodeling associated with honeycomb lung. Further studies are needed to investigate whether this decrease is attributable to collagen absorption.

Keane et al [30] documented high levels of angiogenic cytokines in the bronchoalveolar lavage fluid obtained from patients with early acute respiratory distress syndrome. We demonstrated higher standardized capillary density in the alveolar wall in the exudative stage in our specimens. In low-grade fibrosis in idiopathic pulmonary fibrosis, CD34$^+$ capillaries were increased in the alveolar wall [31]. In fibrogenic pulmonary disorders, capillary angiogenesis may occur in the early phase, possibly contributing to the fibrogenesis. On the other hand, CD34$^+$ capillaries were barely detectable in the fibroblastic foci in idiopathic pulmonary fibrosis [31-33]. We demonstrated that the intra-alveolar fibrotic lesions of DAD included few CD34$^+$ capillaries. In contrast, Masson's body—an organized fibrotic lesion that manifests in cryptogenic organizing pneumonia—was observed to contain many capillaries [34]. Cryptogenic organizing pneumonia is reversible; moreover, fibrosis of Masson's body is repairable. Our findings of capillary angiogenesis in DAD are similar to those in idiopathic pulmonary fibrosis. It is interesting to debate whether the absence of capillary angiogenesis in intra-alveolar fibrotic lesions is associated with a poor prognosis in fibrogenic pulmonary disorders.

Unexpectedly, we demonstrated that D2-40$^+$ cells were frequently present on the surface of intra-alveolar fibrotic lesions in the proliferative stage. This heterotopic expression of D2-40 was observed to only a limited extent in the fibrotic

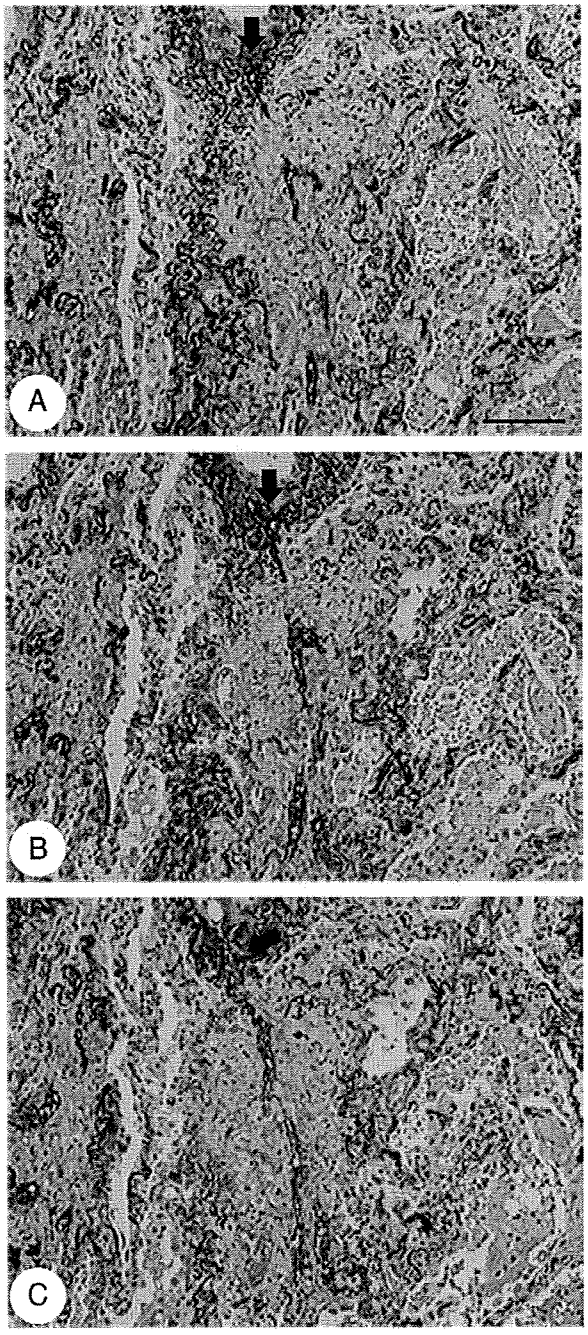

Fig. 6 Connection between newly formed and existing lymphatics in later proliferative stage. Serial sections show that collapsed D2-40$^+$ lumens in intra-alveolar fibrotic lesions connect to an existing one in the later proliferative stage, where alveoli tend to be collapsed. Arrows indicate existing lymphatic vessel around blood vessel. Scale bar, 100 μm.

stage. Analysis of serial tissue sections confirmed that these cells express VEGFR-3, an essential growth factor receptor for lymphatic endothelial cells, whereas these cells did not express the epithelial marker AE1/AE3, demonstrating the character of lymphatic endothelial cells. Furthermore, 3-D reconstructions of serial D2-40-stained sections clearly depicted continuity between these heterotopic and usual lymphatic structures in the intra-alveolar fibrotic lesions. The function of the open structure of lymphatics in DAD remains unknown. Some newly formed lymphatics in the intra-alveolar fibrotic lesions had no connection with the existing lymphatics, suggesting a unique mode of lymphangiogenesis in DAD that differs from the sprouting mode detectable as the conventional process in inflammation.

In conclusion, during the progression of idiopathic DAD, lymphangiogenesis occurs independent of capillary angiogenesis. Understanding the roles of capillary angiogenesis and lymphangiogenesis in pulmonary fibrosis may contribute to recognition of new treatment strategies for aberrant tissue repair.

Acknowledgments

We would like to thank Dr Keiichi Saito, Mrs Naoko Shibata, Mr Koichi Sato, and Dr Toshio Kumasaka for their excellent help.

References

[1] Travis WD, Colby TV, Koss MN, et al. Non-neoplastic disorders of the lower respiratory tract. In: West King D, editor. Atlas of non-tumor pathology. Washington, DC: American Registry of Pathology and Armed Forces Institute of Pathology; 2002. pp. 89-106.
[2] Bachofen M, Weibel ER. Alterations of the gas exchange apparatus in adult respiratory insufficiency associated with septicemia. Am Rev Respir Dis 1977;116:589-615.
[3] Gould VE, Tosco R, Wheelis RF, et al. Oxygen pneumonitis in man: ultrastructural observations on the development of alveolar lesions. Lab Invest 1972;26:499-508.
[4] Katzenstein AL, Bloor CM, Leibow AA. Diffuse alveolar damage—the role of oxygen, shock, and related factors. A review. Am J Pathol 1976;85:209-28.
[5] Katzenstein AL, Myers JL, Mazur MT. Acute interstitial pneumonia: a clinicopathologic, ultrastructural, and cell kinetic study. Am J Surg Pathol 1986;10:256-67.
[6] Sugiyama K, Kawai T. Diffuse alveolar damage and acute interstitial pneumonitis: histochemical evaluation with lectins and monoclonal antibodies against surfactant apoprotein and collagen type IV. Mod Pathol 1993;6:242-8.
[7] Bouros D, Nicholson AC, Polychronopoulos V, et al. Acute interstitial pneumonia. Eur Respir J 2000;15:412-8.
[8] Bonaccorsi A, Cancellieri A, Chilosi M, et al. Acute interstitial pneumonia: report of a series. Eur Respir J 2003;21:187-91.
[9] Olson J, Colby TV, Elliott CG. Hamman-Rich syndrome revisited. Mayo Clin Proc 1990;65:1538-48.
[10] Selman M, King TE, Pardo A, American Thoracic Society, European Respiratory Society, American College of Chest Physicians. Idiopathic pulmonary fibrosis: prevailing and evolving hypotheses about its pathogenesis and implications for therapy. Ann Intern Med 2001;134:136-51.
[11] Munger JS, Huang X, Kawakatsu H, et al. The integrin alpha v beta 6 binds and activates latent TGF beta 1: a mechanism for regulating pulmonary inflammation and fibrosis. Cell 1999;96:319-28.

[12] Adamson IY, Young L, Bowden DH. Relationship of alveolar epithelial injury and repair to the induction of pulmonary fibrosis. Am J Pathol 1988;130:377-83.
[13] Ji RC. Characteristics of lymphatic endothelial cells in physiological and pathological conditions. Histol Histopathol 2005;20:155-75.
[14] Kaipainen A, Korhonen J, Mustonen T, et al. Expression of the fms-like tyrosine kinase 4 gene becomes restricted to lymphatic endothelium during development. Proc Natl Acad Sci USA 1995;92:3566-70.
[15] Banerji S, Ni J, Wang SX, et al. LYVE-1, a new homologue of the CD44 glycoprotein, is a lymph-specific receptor for hyaluronan. J Cell Biol 1999;144:789-801.
[16] Breiteneder-Geleff S, Soleiman A, Kowalski H, et al. Angiosarcomas express mixed endothelial phenotypes of blood and lymphatic capillaries: podoplanin as a specific marker for lymphatic endothelium. Am J Pathol 1999;154:385-94.
[17] Petrova TV, Makinen T, Makela TP, et al. Lymphatic endothelial reprogramming of vascular endothelial cells by the Prox-1 homeobox transcription factor. EMBO J 2002;21:4593-9.
[18] Kahn HJ, Bailey D, Marks A. Monoclonal antibody D2-40, a new marker of lymphatic endothelium, reacts with Kaposi's sarcoma and a subset of angiosarcomas. Mod Pathol 2002;15:434-40.
[19] Williams CS, Leek RD, Robson AM, et al. Absence of lymphangiogenesis and intratumoural lymph vessels in human metastatic breast cancer. J Pathol 2003;200:195-206.
[20] Skobe M, Hawighorst T, Jackson DG, et al. Induction of tumor lymphangiogenesis by VEGF-C promotes breast cancer metastasis. Nat Med 2001;7:192-8.
[21] Pepper MS, Tille JC, Nisato R, et al. Lymphangiogenesis and tumor metastasis. Cell Tissue Res 2003;314:167-77.
[22] Paavonen K, Puolakkainen P, Jussila L, et al. Vascular endothelial growth factor receptor-3 in lymphangiogenesis in wound healing. Am J Pathol 2000;156:1499-504.
[23] Ji RC, Miura M, Qu P, et al. Expression of VEGFR-3 and 5'-nase in regenerating lymphatic vessels of the cutaneous wound healing. Microsc Res Tech 2004;64:279-86.
[24] Maeda S, Suzuki S, Suzuki T, et al. Analysis of intrapulmonary vessels and epithelial-endothelial interactions in the human developing lung. Lab Invest 2002;82:293-301.
[25] Weibel ER. Stereological methods. Volume 1. Practical methods for biological morphometry. Orlando (Fla): Academic Press; 1979. pp. 26-39.
[26] Yamaguchi M, Takahashi T, Togashi H, et al. The corrected collagen content in paraquat lungs. Chest 1986;90:251-7.
[27] Yaegashi H, Takahashi T, Kawasaki M. Microcomputer-aided reconstruction: a system designed for the study of 3-D microstructure in histology and histopathology. J Microsc 1987;146:55-65.
[28] Baluk P, Tammela T, Ator E, et al. Pathogenesis of persistent lymphatic vessel hyperplasia in chronic airway inflammation. J Clin Invest 2005; 115:247-57.
[29] Matsui K, Nagy-Bojarsky K, Laakkonen P, et al. Lymphatic microvessels in the rat remnant kidney model of renal fibrosis: aminopeptidase p and podoplanin are discriminatory markers for endothelial cells of blood and lymphatic vessels. J Am Soc Nephrol 2003;14:1981-9.
[30] Keane MP, Donnelly SC, Belperio JA, et al. Imbalance in the expression of CXC chemokines correlates with bronchoalveolar lavage fluid angiogenic activity and procollagen levels in acute respiratory distress syndrome. J Immunol 2002;169:6515-21.
[31] Ebina M, Shimizukawa M, Shibata N, et al. Heterogeneous increase in CD34-positive alveolar capillaries in idiopathic pulmonary fibrosis. Am J Respir Crit Care Med 2004;169:1203-8.
[32] Renzoni EA, Walsh DA, Salmon M, et al. Interstitial vascularity in fibrosing alveolitis. Am J Respir Crit Care Med 2003;167:438-43.
[33] Cosgrove GP, Brown KK, Schiemann WP, et al. Pigment epithelium-derived factor in idiopathic pulmonary fibrosis: a role in aberrant angiogenesis. Am J Respir Crit Care Med 2004;170: 242-51.
[34] Lappi-Blanco E, Kaarteenaho-Wiik R, Soini Y, et al. Intraluminal fibromyxoid lesions in bronchiolitis obliterans organizing pneumonia are highly capillarized. Hum Pathol 1999;30:1192-6.

Immunogenetics (2008) 60:599–607
DOI 10.1007/s00251-008-0320-4

ORIGINAL PAPER

Mast cell hyperplasia in the skin of *Dsg4*-deficient hypotrichosis mice, which are long-living mutants of lupus-prone mice

Ming-Cai Zhang · Hiroshi Furukawa · Kazuhiro Tokunaka · Kan Saiga · Fumiko Date · Yuji Owada · Masato Nose · Masao Ono

Received: 14 April 2008 / Accepted: 7 July 2008 / Published online: 2 August 2008

Abstract Desmosomal cadherins are essential cell adhesion molecules expressed in the epidermis. We identified a mutation of a cadherin superfamily member, namely, desmoglein 4 (*Dsg4*), in early onset of death (EOD)^{hage} mice with hypotrichosis. The mutation was induced by the insertion of an early transposon II-β into intron 8 of *Dsg4*. Mast cell hyperplasia was observed in the skin of EOD^{hage} mice. The abnormally expanded population of *lpr* T cells, i.e., CD4$^-$CD8$^-$B220$^+$Thy1.2$^+$ αβT cells, in the splenocytes of EOD mice was reduced in EOD^{hage} mice. Therefore, it was suspected that the long-living mutant EOD^{hage} mice were selected from lupus-prone EOD mice because of their immunological immaturity. These findings clearly indicate that *Dsg4* is an important molecule for the formation of hair follicles and hypothesize that unorganized hyperplastic hair follicles in anagen due to the *Dsg4* mutation provide niches for mast cell precursors in the skin.

Keywords Mast cell · Lupus-prone mouse · Hypotrichosis · Desmoglein 4 · Early transposon

Introduction

The early onset of death (EOD) strain is a recombinant inbred strain established from two autoimmune strains—MRL/lpr and BXSB/yaa. MRL/lpr mice show severe lymphadenopathy and splenomegaly due to abnormal expansion of *lpr* T cells, i.e., CD4$^-$CD8$^-$B220$^+$Thy1.2$^+$ αβT cells (Honda et al. 1999). This abnormality is induced by the *lpr* gene, the mutant *Fas* gene due to the integration

DDBJ accession numbers of the sequences in this article: AB240191, AB240192
MGI accession number of the mutant allele in this article: MGI:3766998

M.-C. Zhang · H. Furukawa · F. Date · M. Ono
Department of Pathology,
Tohoku University Graduate School of Medicine,
Seiryo-machi 2-1, Aoba-ku,
Sendai, Japan 980-8575

M.-C. Zhang
Department of Pathology and Laboratory Medicine,
University of Kansas Medical Center,
Kansas City, KS, USA

H. Furukawa (✉)
Department of Rheumatology, Clinical Research Center
for Allergy and Rheumatology, Sagamihara National Hospital,
National Hospital Organization,
Sagamihara, Japan
e-mail: hfurukawa@mail.tains.tohoku.ac.jp

K. Tokunaka · K. Saiga
Evaluation Team II, Biological Research Group,
Pharmaceutical Research Laboratories, Nippon Kayaku Co., Ltd.,
Tokyo, Japan

Y. Owada
Department of Organ Anatomy,
Yamaguchi University Graduate School of Medicine,
Ube, Japan

M. Nose
Department of Pathology, Ehime University School of Medicine,
Toon, Japan

of an early transposon (ETn; Adachi et al. 1993). BXSB male mice also exhibit the autoimmune diseases because of the *yaa* gene, which results from the translocation of the *Tlr7* gene from the X chromosome to the Y chromosome (Pisitkun et al. 2006). Male EOD mice exhibit the *lpr/lpr* and *yaa/−* genes and show abnormal expansion of *lpr* T cells in the spleen and lymph nodes. EOD mice were established by selection based on the early onset of parental death in every generation. As a result, EOD mice survive for shorter periods than the parental strains because of rapid progressive lupus glomerulonephritis. We found spontaneous mutant EOD mice exhibiting almost complete absence of hairs on the trunk and termed them EOD^{hage} mice since *hage* means hairless in Japanese. These spontaneous mutant mice live longer than parental EOD mice because of delayed onset of lupus glomerulonephritis. These long-living mutant mice were naturally selected in a similar manner to other long-living mutant strains derived from lupus-prone strains showing premature death in our studies (Komori et al. 2006; Yoshida et al. 2006).

Mast cells develop from bone-marrow-derived progenitor cells and are distributed to the skin or the mucosa of the genitourinary, gastrointestinal, and respiratory tracts. Mast cells are one of the inflammatory cells that form the first line of the defense in the skin or the mucosa and proliferate on stimulation by cytokines (Abraham and Malaviya 1997). They are primarily stimulated in response to allergic reactions such as anaphylaxis and asthma, parasitic infections, or wound healing. Mast cell hyperplasia was observed in the tissues showing inflammation, fibrosis, or wound healing (Bischoff and Sellge 2002; Noli and Miolo 2001). It was recently reported that mast cells mediate skin allograft tolerance (Lu et al. 2006) and that hair follicles provide the niche for c-kit^{+} mast cell precursors in the skin (Kumamoto et al. 2003). However, it is still ambiguous how mast cell hyperplasia was generated in the skin.

Desmosomes are cell–cell adhesion junctions found in epithelial tissues, meninges, and myocardiums. They anchor the intermediate filament network to the cell membrane and bridge adjacent cells (Garrod and Chidgey 2007; McGrath and Wessagowit 2005). Desmosomes mainly comprise desmosomal cadherins, the armadillo family, and plakins. Desmosomal cadherins are calcium-dependent type I transmembrane adhesion molecules that comprise desmocollins (Dscs) and desmogleins (Dsgs). Three *Dsc* genes and six *Dsg* genes were located in the same locus on mouse chromosome 18 (Whittock 2003). Recently, it was revealed that mutations in *Dsg4* demonstrated localized autosomal recessive hypotrichosis in humans (OMIM #607903, *607892), mice, and rats (Bazzi et al. 2005; Jahoda et al. 2004; Kljuic et al. 2003; Schweizer 2006). *Dsg4* is specifically expressed in the superficial layers of the epidermis in the skin. In this study, we also revealed that a mutation in *Dsg4* caused hypotrichosis in EOD^{hage} mice.

Materials and methods

Mice

EOD and EOD^{hage} mice were bred under specific pathogen-free conditions in Nippon Kayaku Co. (Tokyo, Japan). MSM mice were kindly provided by Dr. Shiroishi (National Institute of Genetics, Mishima, Japan). One hundred five N_2 mice were generated from female (EOD^{hage} × MSM) F_1 and male EOD^{hage} mice. All the animal experiments adhered to the Tohoku University guidelines for animal experiments.

Histological analysis

All tissues from 6-week-old mice were fixed in 10% formalin in 0.01-M phosphate buffer (pH 7.2), embedded in paraffin, and cut into sections. The sections were stained with hematoxylin and eosin or 0.5% toluidine blue in 0.5 M HCl in order to detect mast cells (Huntley et al. 1985). Mast cell numbers in the dorsal skin, ear, and tongue were calculated. The average mast cell number per 500 μm of dorsal skin or ear section was calculated based on the ten fields observed. The average mast cell number per coronal tongue section was also calculated for two mice. Scale bars is equal to 200 μm. The mast cell numbers were statistically analyzed by unpaired *t* test. Data were presented as mean±SD.

Flow cytometric analysis

Fluorescein isothiocyanate (FITC)- or phycoerythrin (PE)-conjugated Abs to Thy1.2 and CD45R/B220 were purchased from BD Bioscience. Splenocytes were isolated and incubated in diluted fluorescence-conjugated monoclonal antibodies at 4°C for 15 min, then washed twice in phosphate-buffered saline with 3% fetal calf serum, 0.1% sodium azide. Stained cells were analyzed using a FACS-Calibur flow cytometer (BD Bioscience, Franklin Lakes, NJ, USA), as previously described (Komori et al. 2006). Small lymphocytic cells were gated in and analyzed.

Positional cloning of the mutant gene

Genotyping of the 105 N_2 mice was performed with 63 polymorphic microsatellite markers, as listed below. To screen the candidate genes, cDNA and genomic DNA sequencing was performed. Total RNAs were isolated from the dorsal skin of EOD and EOD^{hage} mice, using Trizol (Invitrogen, Carlsbad, CA, USA). cDNAs were synthesized

from 5 μg of total RNA by using Superscript III (Invitrogen), according to the manufacturer's instruction. Reverse-transcription polymerase chain reaction (RT-PCR) and genomic PCR were performed with Ex Taq DNA polymerase (Takara Bio, Otsu, Japan). The PCR products were subjected to the sequencing reaction with the BigDye Terminator v3.1 and analyzed by an ABI Prism 3100 sequencer (Applied Biosystems, Foster City, CA, USA). The sequence primers for exons 8 and 9 of *Dsg4* were C T G G T T G G C A C A A T A C T C C A and GGCTCCTCTCATTCCTCCTC, respectively. The microsatellite markers used in this study were *D1Mit231*, *D1Mit22*, *D1Mit132*, *D1Mit102*, *D1Mit115*, *D2Mit365*, *D2Mit522*, *D2Mit224*, *D2Mit102*, *D2Mit282*, *D2Mit200*, *D3Mit224*, *D3Mit230*, *D3Mit101*, *D3Mit147*, *D4Mit286*, *D4Mit197*, *D4Mit186*, *D4Mit251*, *D4Mit131*, *D5Mit381*, *D5Mit197*, *D5Mit213*, *D5Mit338*, *D6Mit159*, *D6Mit261*, *D6Mit149*, *D7Mit68*, *D7Mit77*, *D7Mit301*, *D8Mit124*, *D8Mit190*, *D8Mit240*, *D8Mit215*, *D8Mit245*, *D9Mit54*, *D9Mit355*, *D9Mit214*, *D10Mit189*, *D10Mit259*, *D10Mit151*, *D11Mit20*, *D11Mit41*, *D11Mit360*, *D11Mit338*, *D12Mit109*, *D12Mit110*, *D12Mit141*, *D13Mit233*, *D13Mit291*, *D14Mit69*, *D14Mit266*, *D15Mit265*, *D15Mit121*, *D16Mit58*, *D17Mit115*, *D17Mit127*, *D18Mit83*, *D18Mit14*, *D18Mit40*, *D18Mit210*, *D19Mit68*, and *D19Mit46*.

Results

Hypotrichosis in EOD^{hage} mice

EOD^{hage} pups developed a scanty growth of short hair, similar to lanugos, on the head and the back, whereas adult

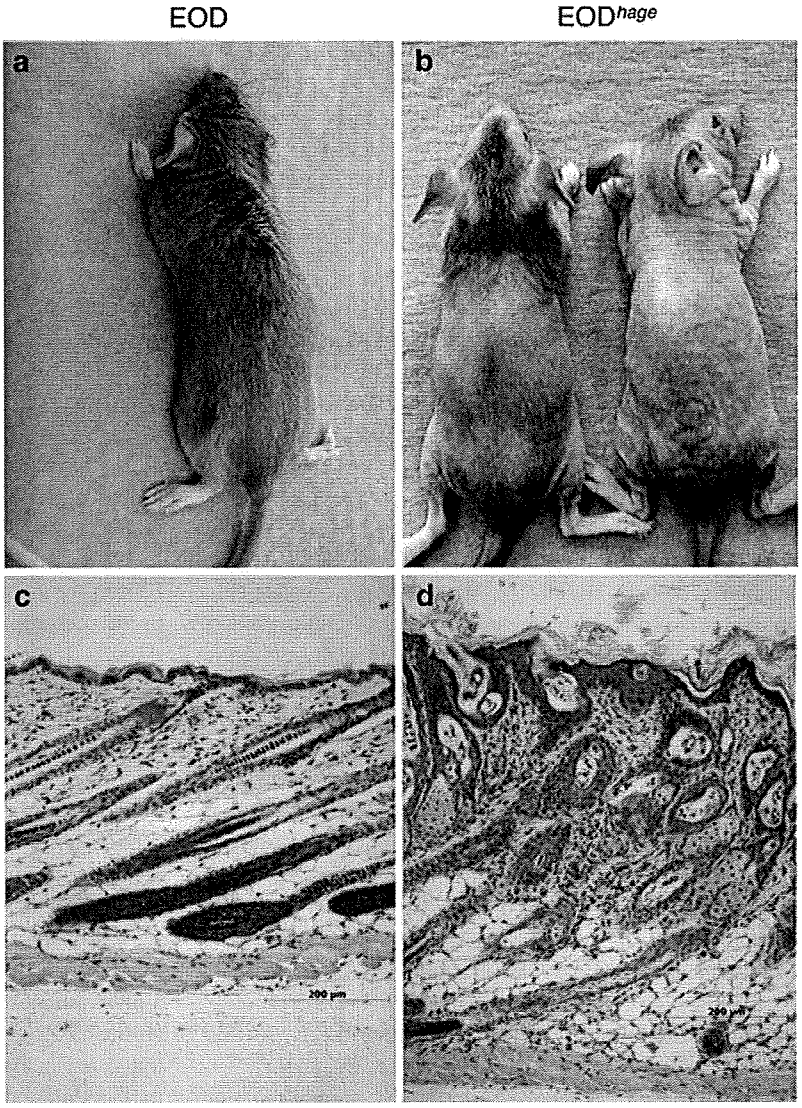

Fig. 1 Phenotype of EOD^{hage} mice. (**a**, **b**) Macroscopic images of 6-week-old wild-type EOD and mutant EOD^{hage} mice. (**c**, **d**) Skin histology (hematoxylin and eosin staining) of the skin of wild-type EOD and EOD^{hage} mice. *Scale bars*: 200 μm

EOD^{hage} mice lost almost all their hair except for that on the parietofrontal skin (Fig. 1b). EOD^{hage} mice also failed to grow vibrissae hairs. The skin of EOD^{hage} mice was thick but vulnerable to injury. Histological analysis of the skin of EOD^{hage} mice showed hyperplasia in the thickened epidermis but not the infiltration of inflammatory cells (Fig. 1d). The axes of hair shafts were randomly oriented, and some were even horizontal to the skin layer and are not parallel with the axis of the body from the head to the tail. More than two hair shafts were observed in a single hair follicle. The numbers of hair follicles seem increased in the skin of EOD^{hage} mice compared with that of EOD mice (Fig. 1c, d). It was difficult to precisely compare the numbers of hair follicles in the sagittal section through skin because the axes of the hair shafts were randomly oriented in the skin of EOD^{hage} mice and the counted number of hair follicles in the sagittal section would not reflect the inner area of hair follicles in the skin. Surprisingly, toluidine blue staining revealed that mast cell accumulation was manifested only in the skin of EOD^{hage} mice, even though mast cell numbers were comparable in the other tissues (Fig. 2). Most of them were accumulated in the superficial layer of the epidermis of EOD^{hage} mice. Thus, the hair follicle abnormality and the mast cell accumulation were observed in the skin of EOD^{hage} mice.

Longer survival of EOD^{hage} mice

EOD^{hage} mice survived significantly longer than EOD mice (Fig. 3a): the median survival time for EOD^{hage} male mice was 99 days, while that for EOD male mice was 88 days. The difference of the median survival time seems short. However, the difference was significant because EOD mice survive much shorter than other lupus-prone strains, as it was named "early onset of death" (Honda et al. 1999). The *lpr*-dependant abnormal T cells, i.e., *lpr* T cells, are fractionated into B220^{+}Thy1.2^{+} double-positive cells. This population is observed in splenocytes from EOD mice and its parental strain, i.e., MRL/lpr mice, since these strains have an *lpr* mutation in the *Fas* gene. However, this population was reduced in the splenocytes of EOD^{hage} mice (Fig. 3b). In addition, the body size of EOD^{hage} mice was relatively smaller than that of EOD mice (data not shown). These data suggest that growth retardation in EOD^{hage} mice results in immunological immaturity, thus delaying the development of *lpr* T cells and the occurrence of glomerulonephritis.

Hypotrichosis is linked to chromosome 18

To gain information regarding the inheritance of this hypotrichotic phenotype of EOD^{hage} mice, F_1 (EOD^{hage} × MSM) mice were generated. All the F_1 mice were not hypotrichotic. Next, N_2 ((EOD^{hage} × SM) ×EOD^{hage}) mice were analyzed. The ratio of wild-type to hypotrichotic mice was approximately 1:1 and sex-related differences were not evident in these N_2 mice (hypotrichosis, 21 female and 26 male mice; wild type, 34 female and 24 male mice), indicating that the hypotrichotic phenotype follows a Mendelian pedigree pattern of autosomal recessive inheritance. One hundred five N_2 mice were analyzed by the genome-wide scan, using the markers described in the "Materials and methods" section. The association between the hypotrichosis phenotype and a microsatellite marker *D18Mit83* on the proximal region of chromosome 18 was defined. High-density polymorphic microsatellite markers were used to define a critical interval between *D18Mit117* and *D18Mit14* (Fig. 4a). This interval comprises five members of the desmosomal cadherin gene family, namely, *Dsg1a*, *Dsg1b*, *Dsg4*, *Dsg3*, *and Dsg2*, located in the same order from the centromere to the telomere. Mutation analysis or gene-targeting studies on *Dsg1a*, *Dsg2*, *Dsg3*, and *Dsg4* were reported. Among them, only the mutation in *Dsg4* was reported to cause hypotrichosis in humans, mice, and rats (Bazzi et al. 2005; Jahoda et al. 2004; Kljuic et al. 2003); moreover, *Dsg4* is expressed only in the mouse skin. Thus, *Dsg4* was the best candidate for the gene responsible for hypotrichosis in EOD^{hage} mice.

ETn in the *Dsg4*^{hage} allele inserts pseudo-exon 8–9 in the transcript

RT-PCR and cDNA sequencing analysis of the *Dsg4* gene in EOD^{hage} mice revealed a 183-bp insertion between exons 8 and 9 (Fig. 4b, c; DNA Databank of Japan (DDBJ) accession number: *AB240191*). This allele and the additional exon in this allele were termed *Dsg4*^{hage} (MGI accession number: *MGI:3766998)* and pseudo-exon 8–9, respectively. In addition, EOD^{hage} mice were renamed EOD-*Dsg4*$^{hage/hage}$ mice. This 183-bp insertion was homologous to other reported ETns, which are integrated into the *lpr*, *whu*, and *tyr* genes for lupus-prone, nude, and albino phenotypes, respectively (Adachi et al. 1993; Hofmann et al. 1998). These 183-bp nucleotides can be translated in frame and can insert 63 amino acids into the extracellular cadherin repeat 3 (EC3) domain of the

Fig. 2 Increased number of mast cells in the dorsal skin of EOD^{hage} mice. (**a**–**h**) Toluidine blue staining of the tissues of wild-type EOD and mutant EOD^{hage} mice. *Scale bars*: 200 μm. **i**–**k** Mast cell numbers in the dorsal skin, ear, and tongue of wild-type EOD and mutant EOD^{hage} mice. The average mast cell numbers per 500 μm of dorsal skin or ear section were calculated based on the ten fields observed. The average mast cell number per coronal tongue section was also calculated for two mice. *Scale bars*: 200 μm. The mast cell number was statistically analyzed by unpaired *t* test. Data were presented as mean±SD

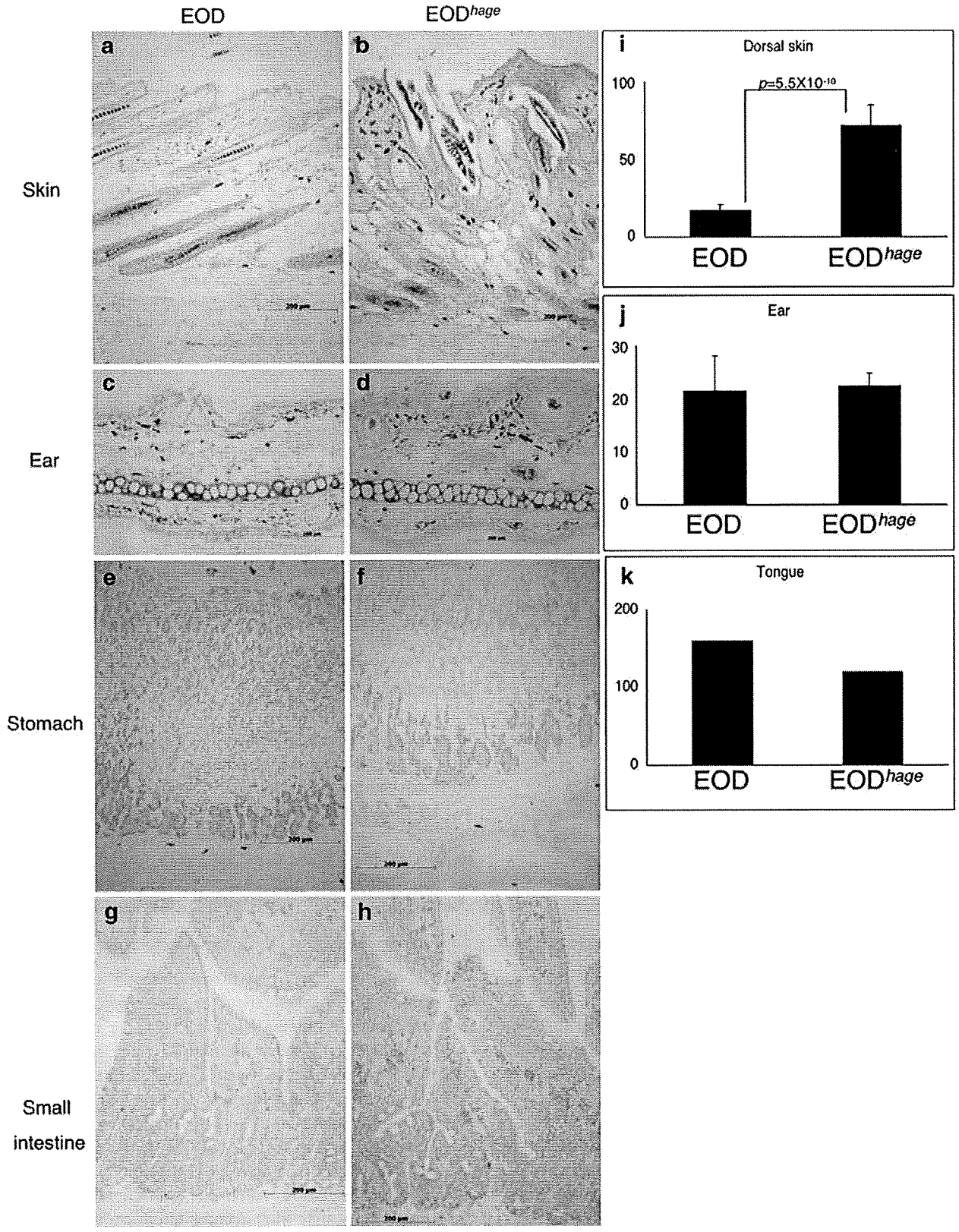
EOD
EOD^hage
Skin
Ear
Stomach
Small intestine
a
b
c
d
e
f
g
h
i
Dorsal skin
p=5.5X10-10
100
50
0
EOD
EOD^hage
j
Ear
30
20
10
0
EOD
EOD^hage
k
Tongue
200
100
0
EOD
EOD^hage

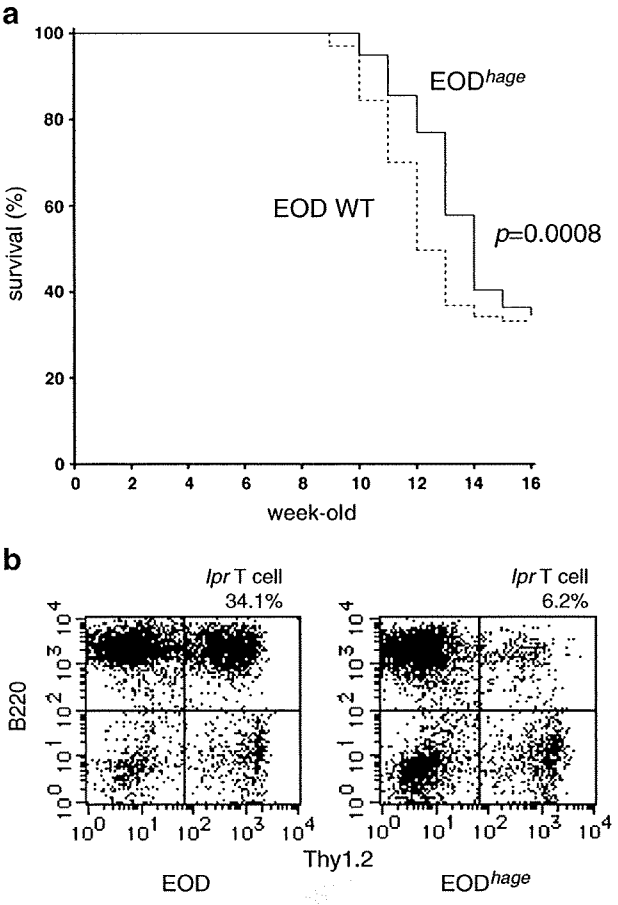

Fig. 3 EOD^{hage} mice show reduced phenotype of autoimmune disease than lupus-prone EOD wild-type mice. **a** The Kaplan–Meier analysis on the survival time of 19 EOD^{hage} male and 69 EOD wild-type male mice. The *p* value was based on the log-rank test. **b** Flow cytometric analysis of *lpr* T cells, i.e., *lpr*-specific B220^{+}Thy1.2^{+} splenocytes, in wild-type EOD and EOD^{hage} mice. Splenocytes were isolated, stained with PE-conjugated anti-B220 and FITC-conjugated anti-Thy1.2 monoclonal antibodies, and analyzed using a FACSCalibur flow cytometer

predicted desmoglein 4 protein (Fig. 4d). *Dsg4* mutations were defined in localized autosomal recessive hypotrichosis patients and its animal models, and most of the mutations occurred in the EC2 or EC3 domain (Messenger et al. 2005; Meyer et al. 2004). These data suggest that the dysfunctional EC3 domain of the Dsg4 protein cannot produce any functional desmosomes in the skin of EOD^{hage} mice.

To determine the genomic structure of this *Dsg4*^{hage} allele, we performed genomic DNA sequencing of intron 8 of the *Dsg4*^{hage} allele. A 5,543-bp ETn II-β was integrated into intron 8, 203 bp away from the initial nucleotide of intron 8 (Fig. 4e; DDBJ accession number: *AB240192*); it was flanked by a duplicated 6-bp repeat (ACTAGG) from the sequence of intron 8 (Fig. 4e, underlined). Pseudo-exon 8–9

Fig. 4 Genetic analysis of *Dsg4*. **a** The hypotrichotic phenotype is linked with the marker *D18Mit83* located at 11.0 cM on chromosome 18. The number of mice with the hypotrichosis haplotype is indicated. The *filled* and *open symbols* indicate homozygotes for the EOD allele and heterozygotes for the EOD and MSM alleles, respectively. **b** RT-PCR analysis of *Dsg4* revealed an insertion of approximately 200 bp between exons 8 and 9 of the *Dsg4*^{hage} allele. RT-PCR was performed using the skin RNA of EOD^{hage} mice with a primer set on exons 8 and 9. **c** The cDNA sequence of the *Dsg4*^{hage} allele contains a 183-bp insert, pseudo-exon 8–9, derived from the early transposon. **d** The amino acid sequence of the EC3 domain from the *Dsg4*^{hage} allele was predicted from **c**. The genomic DNA sequence of the early transposon integrated in intron 8 of the *Dsg4*^{hage} allele. **e** The genomic structure and the splicing from exons 8 and 9 of the *Dsg4*^{hage} allele. The early transposon is represented in *capital letters* and the 5' and 3' flanking 6-bp duplicated sequences from intron 8 of *Dsg4* are *underlined*. **f** The early transposon contains splice acceptor and donor site sequences on both the 5' and 3' sites of pseudo-exon 8–9

was located from 246 to 428 bp of the ETn II-β sequence (Fig. 4f) and flanked by splicing acceptor (AG) and donor (GT) site motifs. The sequence of pseudo-exon 8–9 comprised the nonretroviral sequence and the partial U5 sequence from the 5' long terminal repeat (LTR) of ETn II-β. We found a 98% and 99% similarity between our sequence and the reported ETn II-β sequences in *whu* and *tyr*, respectively, which were found in the SELH strain (Hofmann et al. 1998). Thus, it was indicated that the ETn in the *Dsg4*^{hage} allele inserts pseudo-exon 8–9 in the transcript.

Discussion

In this study, we found a mutation of *Dsg4* gene in EOD^{hage} mice with hypotrichosis. As it was previously reported, *Dsg4* is a causative gene of hypotrichosis in human, mouse, and rat (Bazzi et al. 2005; Jahoda et al. 2004; Kljuic et al. 2003; Schweizer 2006). Since Dsg4 is expressed in the hair follicle and plays an essential role in the differentiation of the hair follicle, we also observed the nonpolarized hair shafts in the skin of EOD^{hage} (Fig. 1d) Based on the report that signals were transduced to keratinocytes via desmosomal cadherins (Fagotto and Gumbiner 1996), it can be deduced that Dsg4 may play a role in signal transduction for regulating the development of the skin with normal polarization of the flumina pilorum.

It is a novel finding that the EOD^{hage} mice used in our experiment manifested mast cell hyperplasia in the superficial layer of the skin epidermis. This finding was never reported in previous studies on *Dsg4* deficiency in human or animal models. The skin of EOD^{hage} mice was thick but vulnerable to injury. Therefore, it is possible that environmental antigens easily reach the superficial layer of epidermis and cause the accumulation of mast cells. However, no significant infiltration of inflammatory cells was observed in the skin of EOD^{hage} mice. The accumu-

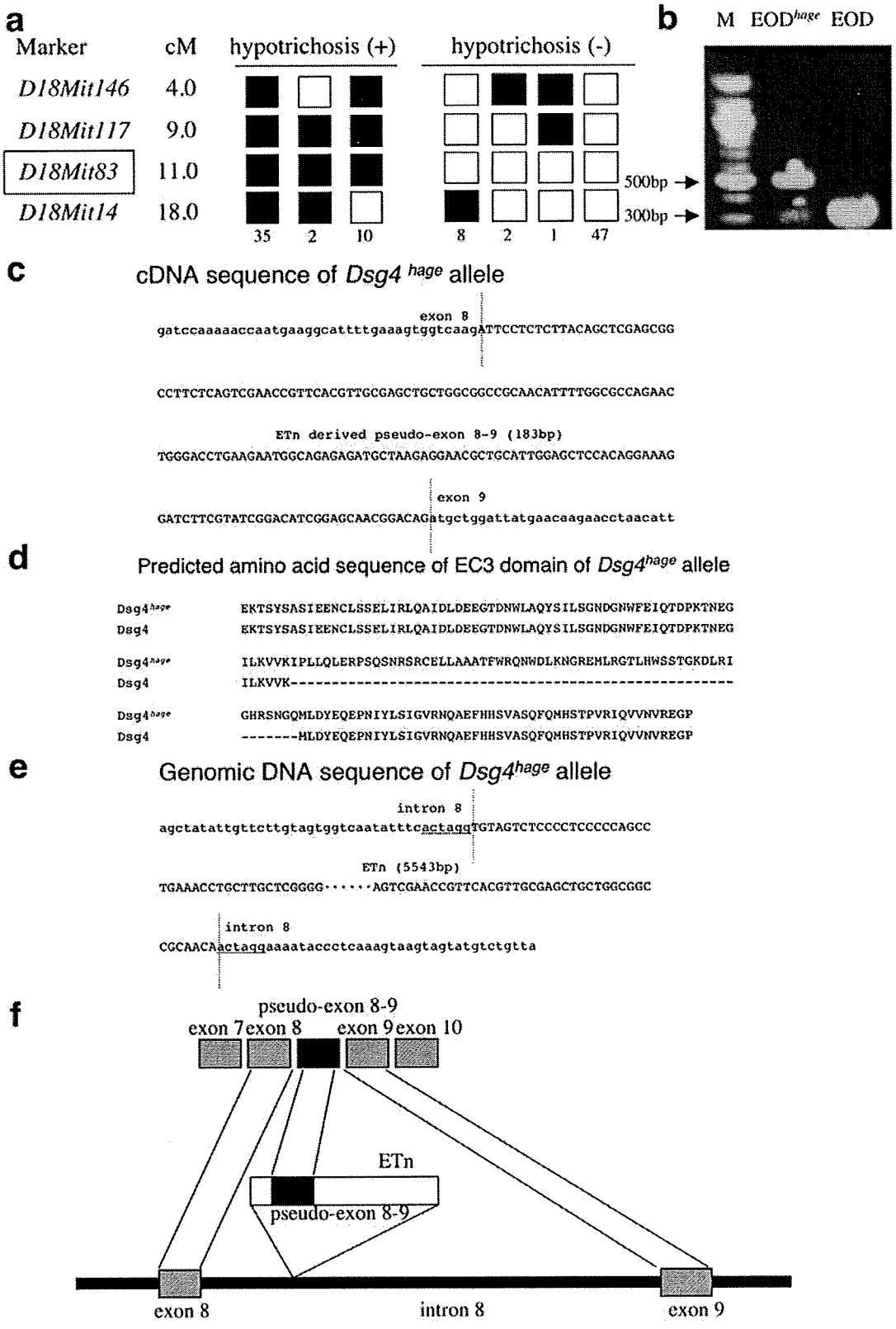
a
Marker
cM
hypotrichosis (+)
hypotrichosis (-)
D18Mit146
4.0
D18Mit117
9.0
D18Mit83
11.0
D18Mit14
18.0
35 2 10
8 2 1 47
b
M EOD^hage EOD
500bp
300bp
c
cDNA sequence of Dsg4 hage allele
exon 8
gatccaaaaaccaatgaaggcattttgaaagtggtcaagATTCCTCTCTTACAGCTCGAGCGG
CCTTCTCAGTCGAACCGTTCACGTTGCGAGCTGCTGGCGGCCGCAACATTTGGCGCCAGAAC
ETn derived pseudo-exon 8-9 (183bp)
TGGGACCTGAAGAATGGCAGAGAGATGCTAAGAGGAACGCTGCATTGGAGCTCCACAGGAAAG
exon 9
GATCTTCGTATCGGACATCGGAGCAACGGACAGatgctggattatgaacaagaacctaacatt
d
Predicted amino acid sequence of EC3 domain of Dsg4hage allele
Dsg4hage EKTSYSASIEENCLSSELIRLQAIDLDEEGTDNWLAQYSILSGNDGNWFEIQTDPKTNEG
Dsg4 EKTSYSASIEENCLSSELIRLQAIDLDEEGTDNWLAQYSILSGNDGNWFEIQTDPKTNEG
Dsg4hage ILKVVKIPLLQLERPSQSNRSRCELLAAATFWRQNWDLKNGREMLRGTLHWSSTGKDLRI
Dsg4 ILKVVK----------
Dsg4hage GHRSNGQMLDYEQEPNIYLSIGVRNQAEFHHSVASQFQMHSTPVRIQVVNVREGP
Dsg4 -------MLDYEQEPNIYLSIGVRNQAEFHHSVASQFQMHSTPVRIQVVNVREGP
e
Genomic DNA sequence of Dsg4hage allele
intron 8
agctatattgttcttgtagtggtcaatatttcactaggTGTAGTCTCCCCTCCCCCAGCC
ETn (5543bp)
TGAAACCTGCTTGCTCGGGG·····AGTCGAACCGTTCACGTTGCGAGCTGCTGGCGGC
intron 8
CGCAACAactaggaaaatacccctcaaagtaagtagtatgtctgtta
f
pseudo-exon 8-9
exon 7 exon 8 exon 9 exon 10
ETn
pseudo-exon 8-9
exon 8
intron 8
exon 9

lation pattern of mast cells in the superficial layer correlates with the expression pattern of *Dsg4*, suggesting that mast cell accumulation can be attributable to the hair follicle abnormality in EOD^{hage} mice. It was previously reported that hair follicles provide c-kit^{+} mast cell precursors and produce stem cell factors (SCFs; Kumamoto et al. 2003). Moreover, the involvement of mast cells in the skin thickness of the tight-skin mouse model of scleroderma was reported (Wang et al. 2005). The association between hair growth and mast cell activation in the skin has been demonstrated with regard to stress-induced hair loss in murine models (Arck et al. 2003). The expression of insulin-like growth factor-1, transforming growth factor-β1, interleukin-15, and SCF in the skin was compared between EOD and EOD^{hage} mice by the real-time RT-PCR method, and no significant difference was observed (data not shown). These data could give rise to a hypothesis that the number of hair follicles in the skin of *Dsg4*-deficient EOD^{hage} mice is increased during anagen and provides more niches for mast cell precursors, leading to mast cell hyperplasia and thickening of the skin. In addition, mast cell hyperplasia in the skin may also contribute to the progression of hypotrichosis. Although the role of mast cells in allergy and anaphylaxis is well known, they also play important protective roles in wound healing and host defense against pathogens (Noli and Miolo 2001; Weller et al. 2006). Further investigations should be conducted to elucidate the mechanism and significance of the accumulated mast cells in the skin of EOD^{hage} mice.

EOD^{hage} mice were significantly long-living mutant mice found in EOD mice. As other long-living mutant mice were derived from lupus-prone strains with short survival time (Komori et al. 2006; Yoshida et al. 2006), EOD^{hage} mice were also effectively selected because it is easy to leave the posterity from long-living mice. In addition, sister–brother mating of EOD mice was continued for the preservation of autosomal recessive and spontaneous mutant genes. EOD^{hage} mice have a lesser number of *lpr* T cells in the spleen compared with EOD mice. Even though *lpr* T cells are not believed to be a pathogenic population with regard to lupus, the number of *lpr* T cells increase as EOD mice age. In addition, EOD^{hage} mice were smaller than EOD mice; however, this phenotype was not reported in any other *Dsg4* mutant mice, rats, or humans. These data suggest that EOD^{hage} mice are relatively immature, thus delaying the occurrence of the autoimmune disease. Since EOD mice die due to the early onset of lupus glomerulonephritis (Honda et al. 1999), the delayed onset of glomerulonephritis in EOD^{hage} mice would make them live longer. We attempted to investigate the cause of the immaturity of EOD^{hage} mice. The expression of growth hormone, prolactin, follicle-stimulating hormone, luteinizing hormone, and adrenocorticotropic hormone in the pituitary gland were comparable in EOD^{hage} mice (data not shown). As *Dsg4* is expressed only in the mouse skin, it was suspected that the expression of the growth hormone receptor or growth-hormone-binding protein is altered in the skin in EOD^{hage} mice. However, the mechanism of immaturity in EOD^{hage} mice is still ambiguous and should be further investigated.

Transposons are mobile DNA sequences that can reposition themselves in different locations within the genome and can cause breaks in the genes. The defined ETn II-β in the present study is a member of mouse LTR retroelements, which form a class of mammalian transposons. Thus far, 16 new germ line mutations in mice have been reported to be caused by the insertion of ETn elements (Baust et al. 2002, 2003). Three of these 16 mutations were induced by the ETn II-β subtype; therefore, sufficient information is available only regarding these three mutations. In our case, the ETn-induced alternative splicing caused insertion of pseudo-exon 8–9 (Fig. 4c, f); however, normally spliced transcripts were also detected in lower amounts (Fig. 4b). Notably, the *Fas* gene mutation in MRL/lpr mice, a maternal strain of the EOD mice, was also induced by the ETn insertion, suggesting that the loss of the function of the *Dsg4*^{hage} allele is due to a relatively common mechanism and that ETn transposition occurs frequently in MRL-derived strains.

The ETn II-β inserted in intron 8 of the *Dsg4*^{hage} allele provides the mutant *Dsg4* mRNA with pseudo-exon 8–9 (Fig. 4b, c), which causes the insertion of 63 amino acids in the EC3 domain of Dsg4 (Fig. 4d). *Dsg4* mutations were defined in localized autosomal recessive hypotrichosis patients and animal models. Most of the mutations occur in the EC2 or EC3 domains (Messenger et al. 2005; Meyer et al. 2004). Based on comparative structural studies of the crystal structure of C-cadherin, EC2 and EC3 domains of Dsg4 are critical for calcium-dependent interaction of desmosomal cadherins. Although it cannot be excluded that the mutant Dsg4 protein from the *Dsg4*^{hage} allele is degraded because of its instability, the 63 amino acids inserted in the EC3 domain may alter the tertiary structure of the Dsg4 protein and disrupt the binding function necessary for intermolecular interaction.

In summary, we report that mast cell hyperplasia was observed in the skin of EOD^{hage} mice with a *Dsg4* mutation due to ETn II-β insertion and that long-living mutant EOD^{hage} mice were selected from the lupus-prone EOD strain because of their immunological immaturity.

Acknowledgements The authors thank Dr. Toshihiko Shiroishi (National Institute of Genetics) for providing MSM mice, Mr. Takuo Hiwatari (Nippon Kayaku Co., Ltd.) and Mr. Kazuumi Kotake (Nippon Kayaku Co., Ltd.) for providing technical assistance in animal experiments, Ms. Naomi Yamaki (Tohoku University) for providing technical assistance in histology, and Ms. Noriko Fujisawa

(Tohoku University) and Ms. Emi Yura (Tohoku University) for secretarial assistance. This study is supported by Grants-in-Aid for Scientific Research from the Ministry of Education, Science, Sports, and Culture of Japan to H.F. (# 16790221) and M.O. (# 16390113, 19390108, and 19659096). The authors declare that the experiments comply with the current laws of Japan.

References

Abraham SN, Malaviya R (1997) Mast cells in infection and immunity. Infect Immun 65:3501–3508

Adachi M, Watanabe-Fukunaga R, Nagata S (1993) Aberrant transcription caused by the insertion of an early transposable element in an intron of the Fas antigen gene of lpr mice. Proc Natl Acad Sci U S A 90:1756–1760 doi:10.1073/pnas.90.5.1756

Arck PC, Handjiski B, Peters EM, Peter AS, Hagen E, Fischer A et al (2003) Stress inhibits hair growth in mice by induction of premature catagen development and deleterious perifollicular inflammatory events via neuropeptide substance P-dependent pathways. Am J Pathol 162:803–814

Baust C, Baillie GJ, Mager DL (2002) Insertional polymorphisms of ETn retrotransposons include a disruption of the wiz gene in C57BL/6 mice. Mamm Genome 13:423–428 doi:10.1007/s00335-002-2178-3

Baust C, Gagnier L, Baillie GJ, Harris MJ, Juriloff DM, Mager DL (2003) Structure and expression of mobile ETnII retroelements and their coding-competent MusD relatives in the mouse insertional polymorphisms of ETn retrotransposons include a disruption of the wiz gene in C57BL/6 mice. J Virol 77:11448–11458 doi:10.1128/JVI.77.21.11448-11458.2003

Bazzi H, Martinez-Mir A, Kljuic A, Christiano AM (2005) Desmoglein 4 mutations underlie localized autosomal recessive hypotrichosis in humans, mice, and rats. J Investig Dermatol Symp Proc 10:222–224 doi:10.1111/j.1087-0024.2005.10110.x

Bischoff SC, Sellge G (2002) Mast cell hyperplasia: role of cytokines. Int Arch Allergy Immunol 127:118–122 doi:10.1159/000048181

Fagotto F, Gumbiner BM (1996) Cell contact-dependent signaling. Dev Biol 180:445–454 doi:10.1006/dbio.1996.0318

Garrod D, Chidgey M (2007) Desmosome structure, composition and function. Biochim Biophys Acta 9:9

Hofmann M, Harris M, Juriloff D, Boehm T (1998) Spontaneous mutations in SELH/Bc mice due to insertions of early transposons: molecular characterization of null alleles at the nude and albino loci. Genomics 52:107–109 doi:10.1006/geno.1998.5409

Honda S, Nemoto K, Mae T, Kinjoh K, Kyogoku M, Kawamura H et al (1999) Mice with early onset of death (EOD) due to lupus glomerulonephritis. Clin Exp Immunol 116:153–163 doi:10.1046/j.1365-2249.1999.00847.x

Huntley JF, Newlands GF, Gibson S, Ferguson A, Miller HR (1985) Histochemical demonstration of chymotrypsin like serine esterases in mucosal mast cells in four species including man. J Clin Pathol 38:375–384 doi:10.1136/jcp.38.4.375

Jahoda CA, Kljuic A, O'Shaughnessy R, Crossley N, Whitehouse CJ, Robinson M et al (2004) The lanceolate hair rat phenotype results from a missense mutation in a calcium coordinating site of the desmoglein 4 gene. Genomics 83:747–756 doi:10.1016/j.ygeno.2003.11.015

Kljuic A, Bazzi H, Sundberg JP, Martinez-Mir A, O'Shaughnessy R, Mahoney MG et al (2003) Desmoglein 4 in hair follicle differentiation and epidermal adhesion: evidence from inherited hypotrichosis and acquired pemphigus vulgaris. Cell 113:249–260 doi:10.1016/S0092-8674(03)00273-3

Komori H, Furukawa H, Mori S, Ito MR, Terada M, Zhang MC et al (2006) A signal adaptor SLAM-associated protein regulates spontaneous autoimmunity and Fas-dependent lymphoproliferation in MRL-Faslpr lupus mice. J Immunol 176:395–400

Kumamoto T, Shalhevet D, Matsue H, Mummert ME, Ward BR, Jester JV et al (2003) Hair follicles serve as local reservoirs of skin mast cell precursors. Blood 102:1654–1660 doi:10.1182/blood-2003-02-0449

Lu LF, Lind EF, Gondek DC, Bennett KA, Gleeson MW, Pino-Lagos K et al (2006) Mast cells are essential intermediaries in regulatory T-cell tolerance. Nature 442:997–1002 doi:10.1038/nature05010

McGrath JA, Wessagowit V (2005) Human hair abnormalities resulting from inherited desmosome gene mutations. Keio J Med 54:72–79 doi:10.2302/kjm.54.72

Messenger AG, Bazzi H, Parslew R, Shapiro L, Christiano AM (2005) A missense mutation in the cadherin interaction site of the desmoglein 4 gene underlies localized autosomal recessive hypotrichosis. J Invest Dermatol 125:1077–1079 doi:10.1111/j.0022-202X.2005.23903.x

Meyer B, Bazzi H, Zidek V, Musilova A, Pravenec M, Kurtz TW et al (2004) A spontaneous mutation in the desmoglein 4 gene underlies hypotrichosis in a new lanceolate hair rat model. Differentiation 72:541–547 doi:10.1111/j.1432-0436.2004.07209007.x

Noli C, Miolo A (2001) The mast cell in wound healing. Vet Dermatol 12:303–313 doi:10.1046/j.0959-4493.2001.00272.x

Pisitkun P, Deane JA, Difilippantonio MJ, Tarasenko T, Satterthwaite AB, Bolland S (2006) Autoreactive B cell responses to RNA-related antigens due to TLR7 gene duplication. Science 312:1669–1672 doi:10.1126/science.1124978

Schweizer J (2006) More than one gene involved in monilethrix: intracellular but also extracellular players. J Invest Dermatol 126:1216–1219 doi:10.1038/sj.jid.5700266

Wang HW, Tedla N, Hunt JE, Wakefield D, McNeil HP (2005) Mast cell accumulation and cytokine expression in the tight skin mouse model of scleroderma. Exp Dermatol 14:295–302 doi:10.1111/j.0906-6705.2005.00315.x

Weller K, Foitzik K, Paus R, Syska W, Maurer M (2006) Mast cells are required for normal healing of skin wounds in mice. FASEB J 20:2366–2368 doi:10.1096/fj.06-5837fje

Whittock NV (2003) Genomic sequence analysis of the mouse desmoglein cluster reveals evidence for six distinct genes: characterization of mouse DSG4, DSG5, and DSG6. J Invest Dermatol 120:970–980 doi:10.1046/j.1523-1747.2003.12257.x

Yoshida M, Saiga K, Hato T, Iwaki S, Niiya T, Arita N et al (2006) Cappuccino mutation in an autoimmune-prone strain of mice suggests a role of platelet function in the progression of immune complex crescentic glomerulonephritis. Arthritis Rheum 54:2934–2943 doi:10.1002/art.22059

厚生労働科学研究費補助金

医療機器開発推進研究事業

ナノバブルと超音波を用いた
高周波超音波三次元画像診断・分子導入システムの開発

平成19年度　総括研究報告書

主任研究者　　小玉　哲也

平成20年 (2008年)　4月

目　次

総　括　研　究　報　告

厚生労働科学研究費補助金（医療機器開発推進研究事業）
平成１９年度　総括研究報告書

ナノバブルと超音波を用いた高周波超音波三次元画像診断・分子デリバリーシステムの開発

課題番号：H19-ナノ-一般-010

主任研究者　小玉　哲也　東北大学先進医工学研究機構

研究要旨：本研究では，ナノバブルと高周波超音波を用いて，三次元画像診断・分子導入システムを開発することを目的とする。EPR効果で腫瘍新生血管から流出・貯留可能な直径200nm以下のナノバブルを作成することができた。 臨床試験導入用動物実験モデルとして肝転移モデル，および所属リンパ節転移モデルの作成をおこなった。 また，腫瘍血管内を流れるバブルの輝度情報を利用した血管抽出法の開発と超音波トリガー法を開発した．がん細胞内への阻害剤導入の導入機序の解明を目指して，非定常・非平衡分子動力学シミュレーションをおこない，膜構造変化と分子導入との関係を明らかにした。

分担研究者

小野栄夫	東北大学大学院医学系研究科・教授
福本　学	東北大学加齢医学研究所・教授
森　士朗	東北大学病院・講師
松村保広	国立がんセンター東病院・部長
藤川重雄	北海道大学大学院工学研究科・教授

A．研究目的

本研究では，超音波造影性薬剤封入型ナノバブルと超音波を用いて，がんの微小血管に特徴的な血管周囲へのバブルの溢出・貯留効果をバブルの軌跡として捉えて三次元画像を構築し，その構築画像の特徴からがんの診断をおこない，同時に輝度の集積